eprints@whiterose.ac.uk
https://eprints.whiterose.ac.uk/

TNF induces increased production of extracellular amyloid-β- and α-synuclein-containing aggregates by human Alzheimer's disease neurons

Daniel R. Whiten[1,†], Philip W. Brownjohn[2†], Steven Moore[2†], Suman De[1], Alessio Strano[2], Yukun Zuo[1], Moritz Haneklaus[2], David Klenerman[1,3,*], Frederick J. Livesey[2*]

1. Department of Chemistry, University of Cambridge, Cambridge CB2 1EW, UK
2. UCL Great Ormond Street Institute of Child Health, Zayed Centre for Research into Rare Disease in Children, 20 Guilford Street, London WC1N 1DZ, UK
3. UK Dementia Research Institute at University of Cambridge, Cambridge CB2 0XY, UK

[†] These authors contributed equally
[*] Correspondence to DK or FJL

Correspondence to: David Klenerman,
Department of Chemistry,
University of Cambridge,
Cambridge CB2 1EW, UK
Email: dk10012@cam.ac.uk

Correspondence may also be sent to: Rick Livesey,
UCL Great Ormond Street Institute of Child Health,
Zayed Centre for Research into Rare Disease in Children,
 20 Guilford Street,
London WC1N 1DZ, UK
Email: r.livesey@ucl.ac.uk

Short title: TNF induces neuron protein aggregate release

Abstract

In addition to increased aberrant protein aggregation, inflammation has been proposed as a key element in the pathogenesis and progression of Alzheimer's disease. How inflammation interacts with other disease pathways and how protein aggregation increases during disease are not clear. We used single molecule imaging approaches and membrane permeabilisation assays to determine the effect of chronic exposure to TNF, a master proinflammatory cytokine, on protein aggregation in human induced pluripotent stem cell-derived neurons harbouring monogenic Alzheimer's disease mutations. We report that exposure of Alzheimer's disease, but not control, neurons to TNF induces substantial production of extracellular protein aggregates. Aggregates from Alzheimer's disease neurons are composed of amyloid-β and α-synuclein and induce significant permeabilisation of lipid membranes in an assay of pathogenicity. These findings provide support for a causal relationship between two crucial processes in Alzheimer's disease pathogenesis, and suggest that targeting inflammation, particularly TNF, may have beneficial downstream effects on ameliorating aberrant protein aggregation and accumulation.

Keywords

Inflammation; protein aggregation; TNF; induced pluripotent stem cells; PSEN1

Abbreviations

AD – Alzheimer's disease

ADPAINT - aptamer DNA points accumulation for imaging in nanoscale topography

Aβ – amyloid-β

CSF – cerebrospinal fluid

iPSC - induced pluripotent stem cell

MCI – mild cognitive impairment

SAVE - single aggregate visualisation by enhancement

TBI – traumatic brain injury

ThT – thioflavin T

TIRF – total internal reflection fluorescence

Introduction

Accumulation of misfolded proteins produced by neurons, initially extracellular deposits of amyloid-β (Aβ), followed by intracellular aggregation of tau, are thought to be primary initiating mechanisms in Alzheimer's disease (AD) pathogenesis (Hardy and Selkoe, 2002; Hardy and Higgins, 1992). Downstream of this biochemical phase of AD are complex interactions between neurons and astrocytes, microglia and other cell types, resulting in chronic neuroinflammation, synaptic dysfunction and eventually widespread cell loss (De Strooper and Karran, 2016). While inflammation in this context has been thought of as a reactive, secondary process, clinical, genetic and experimental evidence now suggests a more central upstream role for immune system involvement in AD pathophysiology and progression (reviewed in (Heneka et al., 2015), although how this initiates is not clear.

Several lines of evidence support the hypothesis that inflammation, either from the disease itself, or derived from secondary insults, augments pathology and cognitive decline in AD. First, increased levels of central and systemic proinflammatory cytokines are observed in mild cognitive impairment and are positively correlated with progression into severe AD (Bermejo et al., 2008; Tarkowski et al., 2003). Second, central neuroinflammation as a result of traumatic brain injury (TBI) speeds deposition of AD-associated proteins and cognitive impairment in animal models (Tajiri et al., 2013; Tran et al., 2011), while a putative epidemiological link has been established between TBI and future risk for AD (Dams-O'Connor et al., 2016). Finally, systemic inflammation is associated with higher levels of circulating proinflammatory cytokines and an increased rate of cognitive decline in AD patients (Dunn et al., 2005; Holmes et al., 2009), and accelerates primary neurodegenerative phenotypes, in particular protein aggregation and deposition, in animal models (Cunningham et al., 2009; Kyrkanides et al., 2011). The mechanisms underlying the relationship between a proinflammatory environment and primary disease phenotypes are yet to be fully elucidated, however.

We and others have reported that cortical excitatory neurons generated *in vitro* from iPSCs derived from individuals carrying disease-causing mutations in amyloid precursor protein (*APP*) or presenilin 1 (*PSEN1*) display robust and reproducible alterations in extracellular Aβ species (Israel et al., 2012; Moore et al., 2015; Yagi et al., 2011), increased tau levels and

phosphorylation (Israel et al., 2012; Moore et al., 2015), the production of synaptotoxic forms of Aβ and tau (Hung and Livesey, 2018). Furthermore, neurons with mutations in *PSEN1* or *APP* have pronounced dysregulation of the endolysosome autophagy network (Hung and Livesey, 2018), with no evidence of intracellular protein aggregation. Modelling of these monogenic, early onset cases of AD in human cellular systems has the potential to inform our understanding of the more common yet complex late onset form of the disease, while allowing for reductionist approaches toward elucidating complex interactions between disease pathways in sensitised genetic backgrounds.

To investigate the relationship between inflammation and protein aggregation in AD, we exposed iPSC-derived AD neurons, which produce higher proportions of aggregation-prone Aβ peptides, to the proinflammatory cytokine TNF, a key mediator common to both central and systemic inflammatory pathways, and measured changes in the production and composition of extracellular aggregates of disease-associated proteins. Using ultra-sensitive single-aggregate imaging techniques (Horrocks et al., 2016; Whiten et al., 2018b) and lipid permeabilisation assays (Flagmeier et al., 2017) capable of characterising the low concentration of secreted aggregates, we show that long-term treatment with TNF substantially increases the production of biologically active Aβ and α-synuclein-containing aggregates specifically in compromised familial AD neurons, but not healthy neurons, suggestive of a role for inflammation in early AD pathology.

Materials and Methods

Generation of human cortical neuron cultures

The iPSC lines used in this study were non-demented control (NDC) and *PSEN1* Intron4 and M146I, as previously reported (Moore et al., 2015). Pluripotent cells were maintained on Geltrex in Essential 8 media (both Thermofisher). With minor modifications to account for feeder free iPSC maintenance, directed differentiation to cerebral cortex was performed as previously described (Shi et al., 2012). Briefly, confluent monolayers of iPSCs were induced to form neural progenitors over the course of 12 days by dual-SMAD inhibition. Cortical progenitors were enriched and then expanded between days 12 and 35 post-neural induction before passaging onto Geltrex coated plates at a density of 80,000 cells per cm^2 for neuronal differentiation and maturation.

TNF treatment

Treatments with recombinant human TNF at 0.1 and 10 ng/ml (Peprotech) or the vehicle control were started 60 days post-neural induction and continued for a duration of 18 d. During this period, a complete exchange of cell culture media was performed every 48 h. The secretomes of neuronal cultures were collected every 6 days, centrifuged at 800 RCF for 3 min to remove cellular debris and stored at -20 °C until required for analysis. For washout experiments, cultures were switched from TNF treatment to the vehicle control after the collection of secretomes at day 12.

Multiplexed Aβ ELISA

Quantification of Aβ38, Aβ40 and Aβ42 was performed with the V-PLEX Aβ peptide Panel 1 kit (K15200E) and a Quickplex SQ120 instrument (MesoScale Discovery) using 25 µl of cell culture supernatant collected at day 18 of TNF treatment.

Gene expression profiling of cortical cultures

To confirm the cortical identity of iPSC-derived neuronal cultures used in every experiment, Trizol-extracted RNA from day 18 vehicle-treated cultures of each genotype was profiled using a custom gene expression panel on the Nanostring platform (Nanostring Technologies). Mean negative control probe counts were subtracted from sample gene counts, before normalisation using the geometric mean of six positive control probes and seven housekeeping genes (*CLTC, GAPDH, GUSB, PPIA, RPLP1, RPS15A, RPS9*).

Cell viability assay

Live imaging of cell viability during the course of TNF treatment was performed by incubating the cultures with NUCLEAR-ID Blue/Red cell viability reagent (Enzo) diluted in culture media for 30 min, according to the manufacturer's instructions. Cultures were washed in fresh media before images were acquired on an Opera Phenix imaging platform (Perkin Elmer) at 37 °C and 5% CO_2. For each timepoint, 37 fields of view were imaged at 20x objective in technical duplicate cultures of each treatment condition, with DAPI (ex375/em435-480) and dsRed (ex561/em570-630) laser and filter sets. For image processing, the number of red nuclei (indicating dead cells) was divided by the number of blue nuclei (indicating total cells) within each field of view to obtain a measure of the proportion of dead nuclei per condition.

TIRF imaging

Imaging of the aggregates was performed using a purpose-built total internal reflection fluorescence (TIRF) microscope. The intensities of 405 nm (Oxxius Laser-Boxx, Oxxius), 488 nm (TOPTICA Photonics) and 561 nm (Cobalt Jive, Cobalt) lasers were first attenuated using neutral density filters, circularly polarised using quarter wave plates, expanded using telescopes and then passed through appropriate filters (FF01-417/60-25 for 405 nm, LL01-488-25 for 488 nm and FF01-561/14-25 for 561 nm, Semrock). The beams were then made concentric using dichroic mirrors (FF552-Di02-25x36 and FF458-Di02-25x36, Semrock) and directed into the back port of an inverted Ti-E Eclipse microscope (Nikon). The light was passed through a 1.49 N.A., 60x TIRF objective. Fluorescence was collected by the same objective, separated from excitation light using dichroic mirror (Di01-R405/488/561/635, Semrock) and passed through filters appropriate for the fluorophore (BLP01-488R-25 for ThT, BLP01-488R-25 for Cal-520 and LP02-568RS-25 for Cy3B, Semrock). The fluorescence was then expanded using a 2.5x relay lens and focussed onto an electron-multiplying charge-coupled device for imaging.

ADPAINT and SAVE imaging was performed as described previously (Whiten et al., 2018b). Briefly, round 50 mm slides first were cleaned under argon plasma (PDC-002, Harrick Plasma) for one hour. A CultureWell coverslip (CultureWell CWCS-50R-1.0, 50 channels) was then cut in half and layered on the slide to create individual wells. Each well was then incubated in aspartic acid (1 mg/ml) for 1 h to create a surface electrostatically unfavourable

to DNA binding. The chambers were then rinsed with PBS, pH 7.4, 0.02 μm filtered (Anotop25, Whatman) and the solution containing aggregates to be imaged incubated in the wells for 5 min. For ADPAINT and SAVE imaging the cell culture media samples were first diluted 1:10 in PBS. The solution was then aspirated and replaced with imaging solution, containing 100 nM aptamer, 1 nM Cy3B-conjugated imaging strand and 5 μM ThT in Tris buffer. The chambers were then sealed using another clean coverslip to prevent evaporation. The sequences of the DNA strands are provided in **Table 1**. All DNA strands were diluted in PBS. To prevent user bias when imaging all images were taken in a grid using an automated script (Micro-Manager); exposure time for all frames was 50 ms. 4000 frames were acquired for ADPAINT imaging, for diffraction-limited imaging (including the single vesicle assay) 100 frames were collected. Localisations were identified using the PeakFit ImageJ plugin of the GDSC Single Molecule Light Microscopy package using a signal strength threshold of 100 and a precision threshold of 20 nm. The DBSCAN algorithm in Python 3.7 (sklearn v0.20.1) was used to identify clusters and remove spurious localisations with epsilon = 3 and minimum points threshold = 10. Aggregate lengths were calculated by skeletonisation in Python 3.7 using SciPy v1.1.0. The data analysis is described in detail in (Whiten et al., 2018b).

Membrane permeabilisation assay

The ability of the samples to permeabilise lipid membranes was performed as described previously (Flagmeier et al., 2017). This assay uses the fluorescence of Cal-520-filled vesicles immobilised on the glass coverslide to determine the relative influx of Ca^{2+} caused by the presence of protein aggregates. Cell culture media samples were used undiluted for these experiments and were incubated with the vesicles on the slides for 10 min before imaging. Antibodies/nanobodies were used to determine whether they could inhibit the permeabilisation and were preincubated with the media samples for 10 min at room temperature before incubation on the slide (see **Table 2** for details of nanobodies and antibodies).

Statistical analysis

All statistical analysis was performed using Graphpad Prism 7. Unless otherwise stated, data was analysed with One or Two-way ANOVA, with additional post hoc testing performed using Dunnett's multiple comparison in the case of significant factor effects or interactions. Data shown in Supplementary Figure 3 were analysed using two sample Kolmogorov-Smirnov

tests. Data shown in Figure panels 2B and 2C was analysed by one-sample t-test, comparing washout effects to non-washout effects, which were set to a baseline of 100%. Number of independent experiments is indicated in figure legends.

Data availability

All primary data are provided in Supplementary Table 1.

Results

TNF induces increased secretion of aggregates by human PSEN1 mutant neurons

We and others have reported that human stem cell-derived cortical neurons carrying mutations in *PSEN1* that cause monogenic, familial Alzheimer's disease alter production of extracellular Aβ to longer, more aggregation-prone forms of the peptide (Moore et al., 2015; Yagi et al., 2011). To study the ability of inflammation to modify the production and aggregation of pathogenic proteins, we exposed human iPSC-derived cortical neurons to two different concentrations of TNF over a prolonged treatment period. Cortical neurons from a non-demented control (NDC) (Israel et al., 2012) and individuals carrying two different *PSEN1* mutations (M146I and Intron 4) (Moore et al., 2015) were generated from iPSCs as previously described (Shi et al., 2012). These two *PSEN1* mutations were studied as they capture differing degrees of deficits in endolysosomal function, with the M146I mutation having a more pronounced phenotype, in terms of changes in lysosome size and defects in autophagy (Hung and Livesey, 2018).

Neurons were treated with either a vehicle control or TNF (0.1 ng/ml and 10 ng/ml; henceforth referred to as TNF low and TNF high, respectively). Preliminary experiments found that extracellular aggregates were clearly detected after 10-12 days, and robustly increased after 16-18 days of TNF treatment, therefore, in the experiments reported here, cell culture media were replaced every two days and collected every six days for analysis (Figure 1A). These concentrations cover the physiological range of TNF reported in the human brain in chronic (Mogi et al., 1994) and acute (Waage et al., 1989) neuroinflammatory conditions, although the local concentration of TNF could be higher. The cortical identity of each neuronal differentiation was confirmed by multiplexed transcriptional profiling (Supplementary Figure 1). Data from a comprehensive single cell RNAseq analysis of neurons of each genotype had previously found that neurons express *TNFR1*, with no detectable expression of *TNF* or *TNFR2* (Supplementary Figure 1).

It has previously been demonstrated that TNF can act directly to increase the activity of the *APP* promoter (Ge and Lahiri, 2002), the expression of β-secretase (Yamamoto et al., 2007) and the activity of γ-secretase (Liao et al., 2004), resulting in increased Aβ production (Liao et al., 2004; Yamamoto et al., 2007). To examine the effects of TNF on the APP processing

pathway in human neurons, we analysed their secretomes with multiplexed Aβ ELISAs after the 18-day treatment period. As previously reported (Moore et al., 2015), the ratio of Aβ40/Aβ42 was significantly impacted by genotype, reflecting the impaired γ-secretase activity of *PSEN1* mutant neurons (Figure 1B). However, there was no significant change in the Aβ40/Aβ42 ratio (Figure 1B) or total Aβ (Aβ38 + Aβ40 + Aβ42) production (Figure 1C) in response to TNF exposure, suggesting the APP processing pathway is not altered in this system by this treatment.

In addition to the increased production of longer forms of Aβ peptides, accumulation of extracellular aggregates comprising protein and peptide oligomers is considered an important pathogenic process in Alzheimer's disease (Hardy and Selkoe, 2002; Hardy and Higgins, 1992). Characterisation of the aggregates secreted by IPSC neurons is challenging due to their low concentrations and heterogeneous size distribution, such that bulk biochemical methods cannot be used, due to insufficient sensitivity. We therefore used two complementary biophysical imaging techniques to directly study the effect of TNF exposure on neuronal production of extracellular protein aggregates. Single aggregate visualisation by enhancement (SAVE) (Horrocks et al., 2016) uses thioflavin T (ThT) to enable the diffraction-limited imaging of β-sheet-containing aggregates in secretomes (Figure 1D). By contrast, aptamer DNA points accumulation for imaging in nanoscale topography (ADPAINT) (Whiten et al., 2018b) is a super-resolution technique that uses an oligonucleotide which recognises aggregates of Aβ and α-synuclein (Tsukakoshi et al., 2012) and is visualised by the transient interactions of a complementary imaging strand (Figure 1E).

Analysis of neural secretomes using both techniques revealed no significant difference in aggregate number between control and *PSEN1* mutant neurons before TNF treatment (Supplementary Figure 2). The limit of our resolution is 20nm, which means that aggregates smaller than this size can still be detected but appear as 20 nm. However, the majority of the aggregates found here were larger than 20 nm and thus their size is accurately determined. We observed no significant changes in aggregate number in the secretomes of healthy control neurons following TNF exposure over the 18-day period, compared to vehicle controls, using both SAVE (Figure 1D) and ADPAINT (Figure 1E). In contrast, 18 days of both TNF low and high treatment induced an increase in aggregate production by both *PSEN1* M146I (4-5 fold low and 6 – 9 fold increase high) and Intron 4 (8-9 fold low and 13 – 14 fold increase) neurons

using both imaging techniques (Figure 1D, E) with the high dose TNF treatment increase being statistically significant. These statistically significant increases in extracellular aggregates were not detected until after 18 days of treatment, indicating that this phenotype is dependent upon both the *PSEN1* mutant genotypes employed and long-term exposure to TNF.

In addition to the number of aggregates, the size and conformation of assemblies is a determinant of their potential pathogenicity (Chiti and Dobson, 2017). We therefore used ADPAINT super resolution imaging to investigate changes in the size of individual aggregates in response to TNF exposure. In vehicle treated cultures, we observed that control neurons produce extracellular aggregates primarily between 20 nm (the size limit of the assay) and 50 nm. *PSEN1* mutant neurons produced significantly less aggregates in this size range, instead generating larger aggregates that spanned between 50 and 150 nm (Supplementary Figure 3A). This result correlates with our recent observations of a significant increase in large aggregates (40 – 200 nm) in the CSF of AD patients compared to that of healthy controls using the same assay (De et al., 2019). We observed a significant reduction in the size of aggregates produced specifically by *PSEN1* mutant neurons after TNF exposure, although the magnitude of this effect size is small and does not bring the size distribution of the aggregates back in line with vehicle treated control cultures (Supplementary Figure 3).

Together, these data demonstrate that *PSEN1* mutant neurons produce a comparable number of extracellular aggregates to controls in normal culture conditions, although the size of aggregates from *PSEN1* mutants is significantly larger which means that they secrete a larger mass of aggregates than controls. *PSEN1* mutant neurons specifically increase the production of extracellular aggregates in response to 18 days of TNF high exposure, with a small decrease in aggregate size observed compared to vehicle controls.

Aggregate secretion is not reversible following TNF withdrawal and is not due to cell death
As the effects of TNF on aggregate production were not acute and only observed at day 18 of our assays, we next assessed the requirement for continuous inflammatory stress in the production of this phenotype in a series of washout experiments. Aggregates were measured in the secretomes of cultures either continuously treated with TNF for 18 days or switched to the vehicle control at day 12 for the final six days, with complete media changes every two

days (Figure 2A). Aggregate production at day 18 was not statistically different between neurons continuously treated with either concentration of TNF and those switched to the vehicle control at day 12, when analysed by SAVE (Figure 2B) and ADPAINT (Figure 2C). Therefore, exposure of human *PSEN1* mutant neurons to TNF initiates a process that manifests even after the subsequent removal of the stimulus.

The signalling pathways of TNF in neurons are complex and have been reported to play both neuroprotective and detrimental roles (Probert, 2015). To test the possibility that extracellular aggregates were due to cell death via TNF signalling, we used a live/dead nuclear dye to quantify cell viability in cultures from each genotype across the course of the treatment by high content imaging. Exposure to either low or high doses of TNF had no significant effect on cell death in control (Figure 2D) or *PSEN1* mutant cultures (Figure 2E-F), indicating that reduced cell viability does not contribute to the observed increase in extracellular aggregates following TNF exposure.

Aggregates produced by PSEN1 mutant neurons permeabilise lipid membranes and contain Aβ and α-synuclein

Membrane permeabilisation is a primary mechanism by which extracellular protein aggregates have been hypothesised to confer toxicity (Demuro et al., 2005) by allowing the entry of calcium ions leading to disrupted calcium homeostasis (Dreses-Werringloer et al., 2008). We used an ultrasensitive assay to measure the membrane permeabilisation activity of aggregates generated by human neurons, which we have previously validated with *in vitro* generated aggregates (Whiten et al., 2018a) and those found in CSF samples from AD patients (Drews et al., 2017). This assay quantifies the ability of aggregates to permeabilise the lipid bilayers of immobilised liposomes, permitting the influx of Ca^{2+} and the activation of an enclosed calcium-dependent fluorescent reporter, which is then normalised to ionomycin-mediated lysis (Figure 3A).

Secretomes from vehicle treated control cultures were limited in their ability to permeabilise membranes and TNF did not increase their potency (Figure 3B). Similarly, vehicle treated *PSEN1* M146I (Figure 3C) and Intron 4 mutant secretomes (Figure 3D) were relatively inert in this assay. However, lipid membrane permeabilisation was significantly increased by secretomes from TNF low and high treated *PSEN1* M146I mutant neurons (Figure 3C) and

from TNF high treated *PSEN1* Intron 4 mutant neurons (Figure 3D), compared to their respective vehicle controls. These results correlate with our SAVE and ADPAINT imaging data, and demonstrate that TNF treatment of *PSEN1* mutant neurons, but not non-demented controls, augments the production of extracellular aggregates that have the capacity to permeabilise lipid membranes and hence have a detrimental effect on neurons.

We have previously demonstrated that the composition of protein aggregates with activity in this assay can be directly determined by pre-incubation with candidate neutralising nanobodies and antibodies (De et al., 2019; Drews et al., 2017). Using this approach, the composition of extracellular aggregates was investigated by pre-incubating the secretomes from TNF-treated *PSEN1* mutant neurons with nanobodies or antibodies to Aβ, α-synuclein and tau, all of which form aggregates in neurodegenerative diseases and are released by neurons in culture (Evans et al., 2018; Moore et al., 2015).

Pre-incubation with an Aβ-specific nanobody (Nb3) (Paraschiv et al., 2013) significantly and substantially reduced membrane permeabilisation by TNF-treated AD neuron secretomes from *PSEN1* M146I (reduction of 31.0% ± 1.9%) (Figure 3E) and Intron 4 (reduction of 58.7% ± 2.3%) mutants (Figure 3F). Pre-incubation with an α-synuclein-specific nanobody (NbSyn2) (Iljina et al., 2017) also significantly reduced membrane permeabilisation by the secretomes of TNF-treated *PSEN1* M146I (reduction of 14.2% ± 6.7%) (Figure 3E) and *PSEN1* Intron 4 neurons (reduction of 32.7% ± 0.9%) (Figure 3F) but by a smaller margin than Nb3. In contrast, pre-incubation with two tau-directed antibodies that bind to different epitopes had no significant effect, suggesting that tau does not form or contribute to the toxic aggregates produced under these conditions. Together, these results suggest that TNF augments the secretion of extracellular Aβ and α-synuclein containing aggregates from *PSEN1* mutant neurons that have the capacity to permeabilise lipid membranes.

Discussion

We report here that chronic TNF treatment of human *PSEN1* mutant neurons, but not healthy control neurons, results in increased release of toxic extracellular protein aggregates. Using single molecule imaging techniques and membrane permeabilisation assays, we determined that these aggregates contain Aβ and/or α-synuclein, potentially with other proteins, and have the capacity to permeabilise lipid membranes. We previously observed an increase in the ability of aggregates in CSF to permeabilise membranes with no accompanying change in aggregate number when comparing patients who are mildly cognitively impaired (MCI) and hence at the early stages of developing AD compared to controls (De et al., 2019). Furthermore, using ADPAINT, we found that this increased membrane permeabilisation corresponded with an increase in the proportion of smaller aggregates present in the MCI CSF, similar to the changes observed here in the aggregate size distribution on exposure of mutant neurons to TNF.

Due to the high concentration of peptide required for oligomerisation, it is presumed that Aβ aggregates *in vivo* are formed intracellularly (Friedrich et al., 2010; Hu et al., 2009). In this study, the extracellular concentration of monomeric Aβ42 in *PSEN1* mutant secretomes was not modified by TNF treatment, and never exceeded 20 pM, which is far below the nanomolar concentrations required for fibril formation (Novo et al., 2018), suggesting an intracellular origin for extracellularly detected aggregates. In addition to Aβ, we also determined that α-synuclein was an aggregate constituent, which may be explained by previous observations that Aβ42 has specific interactions with α-synuclein, which can result in bilateral aggregation of each species (Mandal et al., 2006; Masliah et al., 2001). The presence of Aβ and α-synuclein co-aggregates in TNF treated *PSEN1* secretomes also cannot be excluded and has been observed in vitro (Iljina et al., 2018).

The increased release of aggregates following TNF treatment is independent of cell death, suggesting a regulated mechanism of release from genetically vulnerable neurons. We have previously shown that in addition to altered Aβ production, neurons harbouring *PSEN1* mutations have impaired endolysosomal function, which manifests as a pronounced defect in the degradative phase of autophagy (Hung and Livesey, 2018). We hypothesise perturbed proteostasis due to altered endolysosomal trafficking and reduced autophagy may render

neurons susceptible to aberrant aggregate generation and exocytosis in the presence of an additional trigger. How TNF acts as that trigger is currently not clear, but it is notable that TNF-TNFR signalling regulates autophagy in other cell types (Ge et al., 2018) ,which may further aggravate the pre-existing defects in the autophagy-lysosomal network in *PSEN1* mutant neurons, promoting protein aggregation and release.

The aggregate size distribution that we measure for the mutant neurons, exposed to TNF, is notably similar to that we recently measured in MCI and AD CSF (Figure S2C), using the same imaging method (De et al., 2019). This suggests that similar secretion of aggregates occurs in vivo during the development of AD as observed from human neurons in vitro. Increased aggregate secretion may be a major mechanism for neurons to maintain protein homeostasis under stress, as well as a major source of Aβ monomer (Wang et al., 2017).

Higher concentrations of longer protofibrillar aggregates of Aβ, with sizes in the same range as detected in these experiments (40-200 nm), have previously been shown to cause an inflammatory response via TLR4, leading to production of proinflammatory cytokines including TNF (Colvin et al., 2017; Paranjape et al., 2013; Terrill-Usery et al., 2016). A positive cycle of increased secretion of aggregates leading to increased inflammation and production of TNF and other pro-inflammatory cytokines could therefore drive increased production of Aβ aggregates in the AD brain. Therefore, the increase in number of Aβ aggregates that we observe in the presence of TNF treatment provides a plausible mechanism for the three-fold increase in Aβ aggregates deposited in the AD brain over time (Roberts et al., 2017). Future experiments will need to establish if the same increase in number of aggregates occurs in wild-type neurons, as well as mutant neurons, when exposed to TNF over longer times.   In addition to its role as a modulator of systemic and central inflammation, TNF is a key regulator of processes in neuronal development and homeostasis, primarily through signalling via the TNF receptor 1 (TNFR1) on neurons (Santello and Volterra, 2012), which is the only TNF receptor expressed in the human iPSC-derived neurons studied here. It has been demonstrated that TNFR1 signalling can modulate synaptic strength via exocytosis of AMPA receptors (Beattie et al., 2002; Stellwagen et al., 2005), and endocytosis of GABA receptors (Stellwagen et al., 2005), which may point to overlapping pathways involved in trafficking and exocytosis of protein aggregates in already vulnerable AD neurons in this case. Future

studies will be directed towards elucidating the cellular mechanisms linking TNF signalling and the production and release of protein aggregates specifically from AD neurons.

The amyloid cascade hypothesis, which proposes that aggregation of Aβ is the central pathological event in AD pathogenesis (Hardy and Selkoe, 2002; Hardy and Higgins, 1992), has directed clinical efforts to treat the condition over the past several decades. While there have been a number of high profile clinical failures in this domain (Doody et al., 2013; Selkoe, 2019), there remains significant interest in understanding the mechanisms and pathways leading to protein aggregation, which represents a shared pathogenic pathway in many neurodegenerative conditions. It is becoming accepted that in addition to protein aggregation, inflammation is a key element of early AD pathogenesis (Mhatre et al., 2015). In line with this, preclinical and clinical evidence suggests that targeting inflammation - TNF in particular - is a promising therapeutic avenue. In animal models of AD, selective ablation of microglia, the primary source of proinflammatory cytokines in the CNS, or inhibition of TNF signalling, significantly reduces Aβ deposition while rescuing cognitive defects (He et al., 2007; Shi et al., 2011; Sosna et al., 2018). Promising results from epidemiological studies and small scale clinical trials also suggest that exposure to anti-TNF agents reduces incidence or severity of AD in humans, though there is scope for future large scale randomised clinical trials to confirm these, at times, contradictory results (Ekert et al., 2018).

Having established that TNF promotes protein aggregate production from monogenic AD neurons, which both generate longer, hydrophobic forms of Aβ and have dysfunction of their endolysosomal-autophagy network, a wide range of follow up studies will be of interest. This includes exploring the cellular mechanisms underlying this process, the effect of other AD associated mutations and if similar changes can be observed in the control neuron, if exposed to TNF or a combination of pro-inflammatory cytokines for longer times. It will also be of interest to investigate the potential pro-inflammatory properties of the secreted aggregates and their capability to cause LTP deficit in rodent models.

Overall, our results point to complex interactions during AD initiation *in vivo*, with early stage inflammation, either from the disease itself, or secondary insults, leading to TNF release and subsequent acceleration of the release of protein aggregates, which in turn drives further disease progression. Consequently, directly targeting these aggregates and reducing the

levels of TNF and other inflammatory cytokines are both potential therapeutic targets for slowing AD pathogenesis and may be more effective when used in combination. Finally, studies of iPSC-derived neurons in the presence of chronic levels of TNF may be a more realistic model of AD than studying neurons in the absence of any cellular stress, since the secreted aggregates have similar size distributions to AD CSF and show an increase in number as observed in AD.

COMPETING INTERESTS

The authors declare no competing interests.

REFERENCES

Beattie, E.C., Stellwagen, D., Morishita, W., Bresnahan, J.C., Ha, B.K., Von Zastrow, M., Beattie, M.S., and Malenka, R.C. (2002). Control of synaptic strength by glial TNFalpha. Science *295*, 2282-2285.

Bermejo, P., Martin-Aragon, S., Benedi, J., Susin, C., Felici, E., Gil, P., Ribera, J.M., and Villar, A.M. (2008). Differences of peripheral inflammatory markers between mild cognitive impairment and Alzheimer's disease. Immunol Lett *117*, 198-202.

Chiti, F., and Dobson, C.M. (2017). Protein Misfolding, Amyloid Formation, and Human Disease: A Summary of Progress Over the Last Decade. Annu Rev Biochem *86*, 27-68.

Colvin, B.A., Rogers, V.A., Kulas, J.A., Ridgway, E.A., Amtashar, F.S., Combs, C.K., and Nichols, M.R. (2017). The conformational epitope for a new Abeta42 protofibril-selective antibody partially overlaps with the peptide N-terminal region. *143*, 736-749.

Cunningham, C., Campion, S., Lunnon, K., Murray, C.L., Woods, J.F., Deacon, R.M., Rawlins, J.N., and Perry, V.H. (2009). Systemic inflammation induces acute behavioral and cognitive changes and accelerates neurodegenerative disease. Biol Psychiatry *65*, 304-312.

Dams-O'Connor, K., Guetta, G., Hahn-Ketter, A.E., and Fedor, A. (2016). Traumatic brain injury as a risk factor for Alzheimer's disease: current knowledge and future directions. Neurodegener Dis Manag *6*, 417-429.

De, S., Whiten, D.R., Ruggeri, F.S., Hughes, C., Rodrigues, M., Sideris, D.I., Taylor, C.G., Aprile, F.A., Muyldermans, S., Knowles, T.P.J., *et al.* (2019). Soluble aggregates present in cerebrospinal fluid change in size and mechanism of toxicity during Alzheimer's disease progression. Acta Neuropathologica Communications *7*, 120.

De Strooper, B., and Karran, E. (2016). The Cellular Phase of Alzheimer's Disease. Cell *164*, 603-615.

Demuro, A., Mina, E., Kayed, R., Milton, S.C., Parker, I., and Glabe, C.G. (2005). Calcium dysregulation and membrane disruption as a ubiquitous neurotoxic mechanism of soluble amyloid oligomers. J Biol Chem *280*, 17294-17300.

Doody, R.S., Raman, R., Farlow, M., Iwatsubo, T., Vellas, B., Joffe, S., Kieburtz, K., He, F., Sun, X., Thomas, R.G., *et al.* (2013). A phase 3 trial of semagacestat for treatment of Alzheimer's disease. N Engl J Med *369*, 341-350.

Dreses-Werringloer, U., Lambert, J.-C., Vingtdeux, V., Zhao, H., Vais, H., Siebert, A., Jain, A., Koppel, J., Rovelet-Lecrux, A., Hannequin, D., *et al.* (2008). A Polymorphism in CALHM1 Influences Ca2+ Homeostasis, Aβ Levels, and Alzheimer's Disease Risk. Cell *133*, 1149-1161.

Drews, A., De, S., Flagmeier, P., Wirthensohn, D.C., Chen, W.H., Whiten, D.R., Rodrigues, M., Vincke, C., Muyldermans, S., Paterson, R.W., *et al.* (2017). Inhibiting the Ca(2+) Influx Induced by Human CSF. Cell reports *21*, 3310-3316.

Dunn, N., Mullee, M., Perry, V.H., and Holmes, C. (2005). Association between dementia and infectious disease: evidence from a case-control study. Alzheimer Dis Assoc Disord *19*, 91-94.

Ekert, J.O., Gould, R.L., Reynolds, G., and Howard, R.J. (2018). TNF alpha inhibitors in Alzheimer's disease: A systematic review. Int J Geriatr Psychiatry *33*, 688-694.

Evans, L.D., Wassmer, T., Fraser, G., Smith, J., Perkinton, M., Billinton, A., and Livesey, F.J. (2018). Extracellular Monomeric and Aggregated Tau Efficiently Enter Human Neurons through Overlapping but Distinct Pathways. Cell reports *22*, 3612-3624.

Flagmeier, P., De, S., Wirthensohn, D.C., Lee, S.F., Vincke, C., Muyldermans, S., Knowles, T.P.J., Gandhi, S., Dobson, C.M., and Klenerman, D. (2017). Ultrasensitive Measurement of Ca(2+) Influx into Lipid Vesicles Induced by Protein Aggregates. Angew Chem Int Ed Engl *56*, 7750-7754.

Friedrich, R.P., Tepper, K., Ronicke, R., Soom, M., Westermann, M., Reymann, K., Kaether, C., and Fandrich, M. (2010). Mechanism of amyloid plaque formation suggests an intracellular basis of Abeta pathogenicity. Proc Natl Acad Sci U S A *107*, 1942-1947.

Ge, Y., Huang, M., and Yao, Y.M. (2018). Autophagy and proinflammatory cytokines: Interactions and clinical implications. Cytokine Growth Factor Rev *43*, 38-46.

Ge, Y.W., and Lahiri, D.K. (2002). Regulation of promoter activity of the APP gene by cytokines and growth factors: implications in Alzheimer's disease. Ann N Y Acad Sci *973*, 463-467.

Hardy, J., and Selkoe, D.J. (2002). The amyloid hypothesis of Alzheimer's disease: progress and problems on the road to therapeutics. Science *297*, 353-356.

Hardy, J.A., and Higgins, G.A. (1992). Alzheimer's disease: the amyloid cascade hypothesis. Science *256*, 184-185.

He, P., Zhong, Z., Lindholm, K., Berning, L., Lee, W., Lemere, C., Staufenbiel, M., Li, R., and Shen, Y. (2007). Deletion of tumor necrosis factor death receptor inhibits amyloid beta generation and prevents learning and memory deficits in Alzheimer's mice. J Cell Biol *178*, 829-841.

Heneka, M.T., Carson, M.J., El Khoury, J., Landreth, G.E., Brosseron, F., Feinstein, D.L., Jacobs, A.H., Wyss-Coray, T., Vitorica, J., Ransohoff, R.M.*, et al.* (2015). Neuroinflammation in Alzheimer's disease. Lancet Neurol *14*, 388-405.

Holmes, C., Cunningham, C., Zotova, E., Woolford, J., Dean, C., Kerr, S., Culliford, D., and Perry, V.H. (2009). Systemic inflammation and disease progression in Alzheimer disease. Neurology *73*, 768-774.

Horrocks, M.H., Lee, S.F., Gandhi, S., Magdalinou, N.K., Chen, S.W., Devine, M.J., Tosatto, L., Kjaergaard, M., Beckwith, J.S., Zetterberg, H.*, et al.* (2016). Single-Molecule Imaging of Individual Amyloid Protein Aggregates in Human Biofluids. ACS Chem Neurosci *7*, 399-406.

Hu, X., Crick, S.L., Bu, G., Frieden, C., Pappu, R.V., and Lee, J.M. (2009). Amyloid seeds formed by cellular uptake, concentration, and aggregation of the amyloid-beta peptide. Proc Natl Acad Sci U S A *106*, 20324-20329.

Hung, C.O.Y., and Livesey, F.J. (2018). Altered gamma-Secretase Processing of APP Disrupts Lysosome and Autophagosome Function in Monogenic Alzheimer's Disease. Cell reports *25*, 3647-3660 e3642.

Iljina, M., Dear, A.J., Garcia, G.A., De, S., Tosatto, L., Flagmeier, P., Whiten, D.R., Michaels, T.C.T., Frenkel, D., Dobson, C.M.*, et al.* (2018). Quantifying Co-Oligomer Formation by α-Synuclein. ACS Nano *12*, 10855-10866.

Iljina, M., Hong, L., Horrocks, M.H., Ludtmann, M.H., Choi, M.L., Hughes, C.D., Ruggeri, F.S., Guilliams, T., Buell, A.K., Lee, J.-E.*, et al.* (2017). Nanobodies raised against monomeric α-synuclein inhibit fibril formation and destabilize toxic oligomeric species. BMC Biology *15*, 57.

Israel, M.A., Yuan, S.H., Bardy, C., Reyna, S.M., Mu, Y., Herrera, C., Hefferan, M.P., Van Gorp, S., Nazor, K.L., Boscolo, F.S.*, et al.* (2012). Probing sporadic and familial Alzheimer's disease using induced pluripotent stem cells. Nature *482*, 216-220.

Kyrkanides, S., Tallents, R.H., Miller, J.N., Olschowka, M.E., Johnson, R., Yang, M., Olschowka, J.A., Brouxhon, S.M., and O'Banion, M.K. (2011). Osteoarthritis accelerates and exacerbates Alzheimer's disease pathology in mice. J Neuroinflammation *8*, 112.

Liao, Y.F., Wang, B.J., Cheng, H.T., Kuo, L.H., and Wolfe, M.S. (2004). Tumor necrosis factor-alpha, interleukin-1beta, and interferon-gamma stimulate gamma-secretase-mediated cleavage of amyloid precursor protein through a JNK-dependent MAPK pathway. J Biol Chem *279*, 49523-49532.

Mandal, P.K., Pettegrew, J.W., Masliah, E., Hamilton, R.L., and Mandal, R. (2006). Interaction between Abeta peptide and alpha synuclein: molecular mechanisms in

overlapping pathology of Alzheimer's and Parkinson's in dementia with Lewy body disease. Neurochem Res *31*, 1153-1162.

Masliah, E., Rockenstein, E., Veinbergs, I., Sagara, Y., Mallory, M., Hashimoto, M., and Mucke, L. (2001). beta-amyloid peptides enhance alpha-synuclein accumulation and neuronal deficits in a transgenic mouse model linking Alzheimer's disease and Parkinson's disease. Proc Natl Acad Sci U S A *98*, 12245-12250.

Mhatre, S.D., Tsai, C.A., Rubin, A.J., James, M.L., and Andreasson, K.I. (2015). Microglial malfunction: the third rail in the development of Alzheimer's disease. Trends Neurosci *38*, 621-636.

Mogi, M., Harada, M., Riederer, P., Narabayashi, H., Fujita, K., and Nagatsu, T. (1994). Tumor necrosis factor-alpha (TNF-alpha) increases both in the brain and in the cerebrospinal fluid from parkinsonian patients. Neurosci Lett *165*, 208-210.

Moore, S., Evans, L.D., Andersson, T., Portelius, E., Smith, J., Dias, T.B., Saurat, N., McGlade, A., Kirwan, P., Blennow, K., *et al.* (2015). APP metabolism regulates tau proteostasis in human cerebral cortex neurons. Cell reports *11*, 689-696.

Novo, M., Freire, S., and Al-Soufi, W. (2018). Critical aggregation concentration for the formation of early Amyloid-beta (1-42) oligomers. Sci Rep *8*, 1783.

Paranjape, G.S., Terrill, S.E., Gouwens, L.K., Ruck, B.M., and Nichols, M.R. (2013). Amyloid-beta(1-42) protofibrils formed in modified artificial cerebrospinal fluid bind and activate microglia. Journal of neuroimmune pharmacology : the official journal of the Society on NeuroImmune Pharmacology *8*, 312-322.

Paraschiv, G., Vincke, C., Czaplewska, P., Manea, M., Muyldermans, S., and Przybylski, M. (2013). Epitope structure and binding affinity of single chain llama anti-β-amyloid antibodies revealed by proteolytic excision affinity-mass spectrometry. Journal of Molecular Recognition *26*, 1-9.

Probert, L. (2015). TNF and its receptors in the CNS: The essential, the desirable and the deleterious effects. Neuroscience *302*, 2-22.

Roberts, B.R., Lind, M., Wagen, A.Z., Rembach, A., Frugier, T., Li, Q.X., Ryan, T.M., McLean, C.A., Doecke, J.D., Rowe, C.C., *et al.* (2017). Biochemically-defined pools of amyloid-beta in sporadic Alzheimer's disease: correlation with amyloid PET. Brain : a journal of neurology *140*, 1486-1498.

Santello, M., and Volterra, A. (2012). TNFalpha in synaptic function: switching gears. Trends Neurosci *35*, 638-647.

Selkoe, D.J. (2019). Alzheimer disease and aducanumab: adjusting our approach. Nature Reviews Neurology *15*, 365-366.

Shi, J.Q., Shen, W., Chen, J., Wang, B.R., Zhong, L.L., Zhu, Y.W., Zhu, H.Q., Zhang, Q.Q., Zhang, Y.D., and Xu, J. (2011). Anti-TNF-alpha reduces amyloid plaques and tau phosphorylation and induces CD11c-positive dendritic-like cell in the APP/PS1 transgenic mouse brains. Brain Res *1368*, 239-247.

Shi, Y., Kirwan, P., and Livesey, F.J. (2012). Directed differentiation of human pluripotent stem cells to cerebral cortex neurons and neural networks. Nature protocols *7*, 1836-1846.

Sosna, J., Philipp, S., Albay, R., 3rd, Reyes-Ruiz, J.M., Baglietto-Vargas, D., LaFerla, F.M., and Glabe, C.G. (2018). Early long-term administration of the CSF1R inhibitor PLX3397 ablates microglia and reduces accumulation of intraneuronal amyloid, neuritic plaque deposition and pre-fibrillar oligomers in 5XFAD mouse model of Alzheimer's disease. Mol Neurodegener *13*, 11.

Stellwagen, D., Beattie, E.C., Seo, J.Y., and Malenka, R.C. (2005). Differential regulation of AMPA receptor and GABA receptor trafficking by tumor necrosis factor-alpha. J Neurosci *25*, 3219-3228.

Tajiri, N., Kellogg, S.L., Shimizu, T., Arendash, G.W., and Borlongan, C.V. (2013). Traumatic brain injury precipitates cognitive impairment and extracellular Abeta aggregation in Alzheimer's disease transgenic mice. PLoS One *8*, e78851.

Tarkowski, E., Andreasen, N., Tarkowski, A., and Blennow, K. (2003). Intrathecal inflammation precedes development of Alzheimer's disease. J Neurol Neurosurg Psychiatry *74*, 1200-1205.

Terrill-Usery, S.E., Colvin, B.A., Davenport, R.E., and Nichols, M.R. (2016). Aβ40 has a subtle effect on Aβ42 protofibril formation, but to a lesser degree than Aβ42 concentration, in Aβ42/Aβ40 mixtures. Arch Biochem Biophys *597*, 1-11.

Tran, H.T., LaFerla, F.M., Holtzman, D.M., and Brody, D.L. (2011). Controlled cortical impact traumatic brain injury in 3xTg-AD mice causes acute intra-axonal amyloid-beta accumulation and independently accelerates the development of tau abnormalities. J Neurosci *31*, 9513-9525.

Tsukakoshi, K., Abe, K., Sode, K., and Ikebukuro, K. (2012). Selection of DNA aptamers that recognize alpha-synuclein oligomers using a competitive screening method. Anal Chem *84*, 5542-5547.

Waage, A., Halstensen, A., Shalaby, R., Brandtzaeg, P., Kierulf, P., and Espevik, T. (1989). Local production of tumor necrosis factor alpha, interleukin 1, and interleukin 6 in meningococcal meningitis. Relation to the inflammatory response. J Exp Med *170*, 1859-1867.

Wang, J., Gu, B.J., Masters, C.L., and Wang, Y.-J. (2017). A systemic view of Alzheimer disease — insights from amyloid-β metabolism beyond the brain. Nature Reviews Neurology *13*, 612.

Whiten, D.R., Cox, D., Horrocks, M.H., Taylor, C.G., De, S., Flagmeier, P., Tosatto, L., Kumita, J.R., Ecroyd, H., Dobson, C.M.*, et al.* (2018a). Single-Molecule Characterization of the Interactions between Extracellular Chaperones and Toxic alpha-Synuclein Oligomers. Cell reports *23*, 3492-3500.

Whiten, D.R., Zuo, Y., Calo, L., Choi, M.L., De, S., Flagmeier, P., Wirthensohn, D.C., Kundel, F., Ranasinghe, R.T., Sanchez, S.E.*, et al.* (2018b). Nanoscopic Characterisation of Individual Endogenous Protein Aggregates in Human Neuronal Cells. Chembiochem : a European journal of chemical biology *19*, 2033-2038.

Yagi, T., Ito, D., Okada, Y., Akamatsu, W., Nihei, Y., Yoshizaki, T., Yamanaka, S., Okano, H., and Suzuki, N. (2011). Modeling familial Alzheimer's disease with induced pluripotent stem cells. Human molecular genetics *20*, 4530-4539.

Yamamoto, M., Kiyota, T., Horiba, M., Buescher, J.L., Walsh, S.M., Gendelman, H.E., and Ikezu, T. (2007). Interferon-gamma and tumor necrosis factor-alpha regulate amyloid-beta plaque deposition and beta-secretase expression in Swedish mutant APP transgenic mice. Am J Pathol *170*, 680-692.

FIGURE LEGENDS

Figure 1. TNF induces production of extracellular aggregates by human *PSEN1* mutant neurons

(A) iPSC-derived neurons were exposed to TNF or vehicle for 18 days, with media collected every six days for analysis. (B) ELISA measurements of extracellular Aβ revealed a significant impact of genotype, but not chronic TNF treatment, on Aβ40/Aβ42 ratio (Two-way ANOVA; Genotype factor $F_{(2, 15)}$ = 28.32, p<0.0001, Treatment factor $F_{(2, 15)}$ = 1.024, p > 0.05, Interaction $F_{(4, 15)}$ = 0.04128, p > 0.05). (C) Similarly, there was no significant dose-dependent change in total extracellular Aβ (Aβ38 + Aβ40 + Aβ42) as a result of chronic TNF exposure (Two-way ANOVA; Genotype factor $F_{(2, 9)}$ = 1.467, p > 0.05, Treatment factor $F_{(1, 9)}$ = 1.010, p > 0.05, Interaction $F_{(2, 9)}$ = 0.7066, p > 0.05). (D) SAVE imaging allows the imaging and quantification of individual ThT-positive β-sheet containing aggregates from neural secretomes. SAVE imaging of control secretomes revealed no effect of TNF on aggregate number (Two-way ANOVA; Time factor $F_{(2, 15)}$ = 4.188, p < 0.05, Treatment factor $F_{(2, 15)}$ = 1.350, p > 0.05, Interaction $F_{(4, 15)}$ = 1.161, p > 0.05, all multiple comparisons p > 0.05). By contrast, high dose TNF significantly increased the number of aggregates in the secretomes of *PSEN1* M146I (Two-way ANOVA; Time factor $F_{(2, 15)}$ = 18.60, p < 0.0001, Treatment factor $F_{(2, 15)}$ = 4.048, p < 0.05, Interaction $F_{(4, 15)}$ = 2.321, p > 0.05) and Intron 4 (Two-way ANOVA; Time factor $F_{(2, 15)}$ = 7.943, p < 0.01, Treatment factor $F_{(2, 15)}$ = 2.752, p > 0.05, Interaction $F_{(4, 15)}$ = 1.536, p > 0.05) mutant neuronal cultures. (E) ADPAINT imaging uses aptamers that recognise Aβ and α-synuclein oligomers, which transiently interact with complementary imaging strands to enable detection of aggregates using super resolution microscopy. ADPAINT imaging of the same secretomes confirmed that TNF had no effect on the production of aggregates from control neurons (Two-way ANOVA; Time factor $F_{(2, 15)}$ = 1.217, p > 0.05, Treatment factor $F_{(2, 15)}$ = 0.8401, p > 0.05, Interaction $F_{(4, 15)}$ = 0.03294, p > 0.05), however high doses resulted in a significant increase in aggregates produced by *PSEN1* M146I (Two-way ANOVA; Time factor $F_{(2, 15)}$ = 22.38, p < 0.0001, Treatment factor $F_{(2, 15)}$ = 3.819, p < 0.05, Interaction $F_{(4, 15)}$ = 2.424, p > 0.05) and Intron 4 (Two-way ANOVA; Time factor $F_{(2, 15)}$ = 11.15, p < 0.01, Treatment factor $F_{(2, 15)}$ = 2.609, p > 0.05, Interaction $F_{(4, 15)}$ = 1.838, p > 0.05) mutant neurons. Data in D,E are represented as a fold change in aggregate number from day 0 baseline. N = 3 independent

experiments in all cases. Error bars represent S.D. In D-E * = p < 0.05, ** = p < 0.01 versus vehicle control, Dunnett's multiple comparisons.

Figure 2. Augmented extracellular aggregate production continues following TNF withdrawal and is not due to increased cell death

(A) TNF was removed at day 12 of treatment by switching a subset of cultures to the vehicle control, with media changed every two days to ensure complete washout. SAVE (B) and ADPAINT (C) imaging of secretomes subjected to TNF removal and washout at day 12 revealed comparable number of aggregates to those cultures treated for a full 18 days (One sample t test vs. 100%, p > 0.05 in all cases). (D – F) High content imaging revealed no significant changes in cell viability in control (D) (Two-way Repeated-measures ANOVA; Time factor $F_{(3, 9)}$ = 3.966, p < 0.05, Treatment factor $F_{(2, 3)}$ = 0.09118, p > 0.05, Interaction $F_{(6, 9)}$ = 0.3276, p > 0.05, all multiple comparisons p > 0.05), *PSEN1* M146I (E) (Two-way Repeated-measures ANOVA; Time factor $F_{(3, 9)}$ = 1.554, p > 0.05, Treatment factor $F_{(2, 3)}$ = 4.394, p > 0.05, Interaction $F_{(6, 9)}$ = 0.09461, p > 0.05) or Intron 4 (F) (Two-way Repeated-measures ANOVA; Time factor $F_{(3, 9)}$ = 3.092, p > 0.05, Treatment factor $F_{(2, 3)}$ = 0.03124, p > 0.05, Interaction $F_{(6, 9)}$ = 0.2670, p > 0.05) mutant neurons as a result of TNF treatment when assessed by cell viability dye. Data in B and C are represented as a percentage of the aggregate number in washout conditions at day 18 compared with continuous 18-day TNF treatment in each case. N = 2 independent experiments in all assays. Error bars represent S.D.

Figure 3. Aggregates are composed of Aβ and α-synuclein and permeabilise lipid membranes

(A) The single-vesicle permeabilisation assay consists of a preparation of liposomes loaded with a fluorescent Ca^{2+} detection dye (Cal-520), which fluoresce after protein aggregates disrupt the membrane and allow the entry of Ca^{2+}. Ionomycin induces maximal permeabilisation and is used to benchmark liposome responses to aggregates as a percentage of total possible Ca^{2+} influx. (B – D) Exposure of liposomes to day 18 treated neural secretomes revealed that secretomes from control neurons (B) did not induce permeabilisation of liposomes (One-way ANOVA; $F_{(2, 5)}$ = 0.8862, p > 0.05), but those from TNF-treated *PSEN1* M146I (C) (One-way ANOVA; $F_{(2, 5)}$ = 30.87, p < 0.01) and Intron 4 (D) (One-way ANOVA; $F_{(2, 5)}$ = 22.49, p < 0.01) mutant neurons induced significant liposome

disruption, consistent with the presence of increased numbers of protein aggregates. (E, F) Pre-incubation of TNF high-treated neural secretomes with nanobodies to Aβ (Nb3) and α-synuclein (NbSyn2) significantly reduced the permeabilisation potential of the secretomes from *PSEN1* M146I (E) (One-way ANOVA; $F_{(5, 6)} = 36.25$, $p < 0.001$) and Intron 4 (F) (One-way ANOVA; $F_{(5, 6)} = 162.1$, $p < 0.0001$) mutant neurons, while pre-incubation with control IgG or two tau-directed antibodies (Tau 5 and HT7) had no significant effect. N = 3 independent experiments in B-D, and N = 2 independent liposome preparations in E-F. Error bars represent S.D. In B-D, * = $p < 0.05$ and ** = $p < 0.01$ versus vehicle treatment, Dunnett's multiple comparisons. In E-F * = $p < 0.05$, *** = $p < 0.001$ and **** = $p < 0.0001$ versus no antibody preincubation, Dunnett's multiple comparisons.
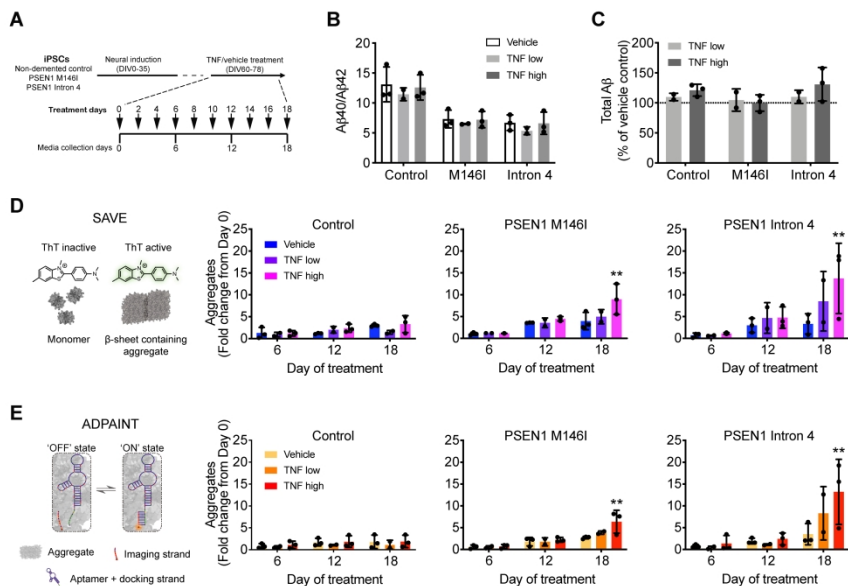
Figure 1. TNF induces production of extracellular aggregates by human PSEN1 mutant neurons

316x183mm (300 x 300 DPI)
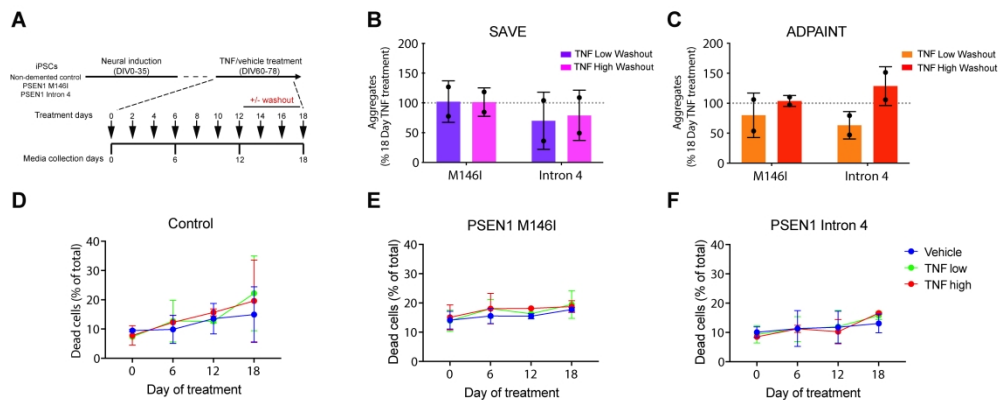
Figure 2. Augmented extracellular aggregate production continues following TNF withdrawal and is not due to increased cell death
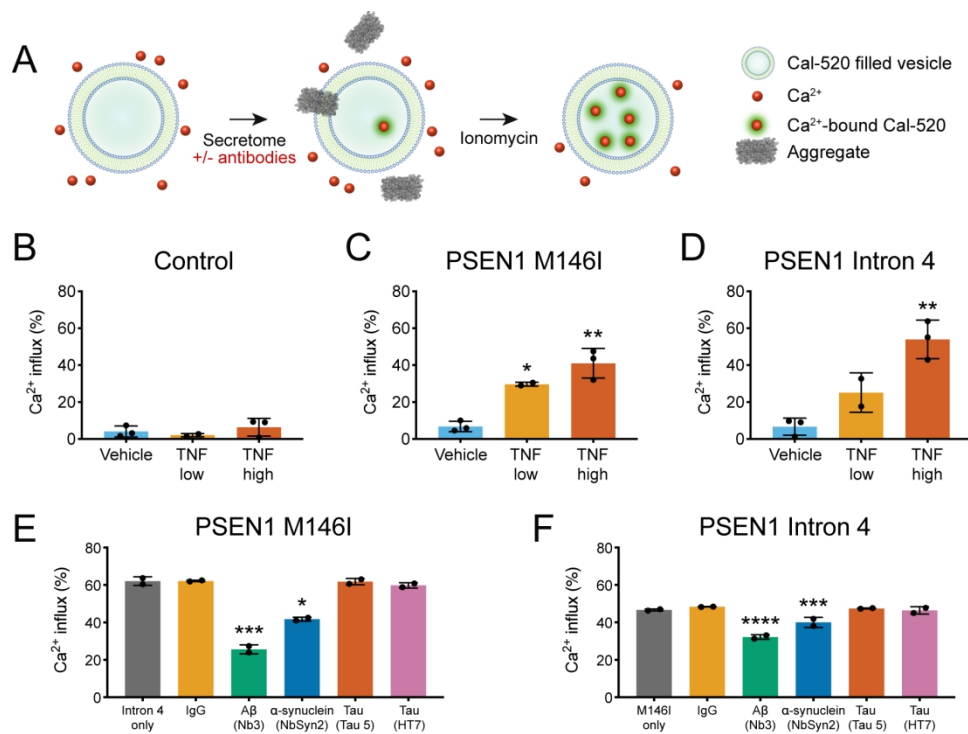
Figure 3. Aggregates are composed of Aβ and α-synuclein and permeabilise lipid membranes

166x121mm (300 x 300 DPI)

Table 1: Sequences of DNA constructs used in this work.

DNA strand name	Sequence
Aptamer + linker + docking strand	GCCTGTGGTGTTGGGGCGGGTGCGTTATACATCTA
Imaging strand	CCAGATGTAT-CY3B

Table 2: Antibodies and nanobodies used in single vesicle assays.

Antibody	Target	Supplier	Concentration used
NB3	Amyloid-β	Prof. Serge Muyldermans, Vrije Universiteit Brussel, Belgium	300 nM
NBSyn2	α-synuclein	Dr Marija Iljina, University of Cambridge, UK	300 nM
HT7	Tau	Thermo Fisher Scientific (MN1000)	300 nM
Tau-5	Tau	Abcam (ab3931)	300 nM
IgG control	N/A	Abcam (ab6556)	300 nM
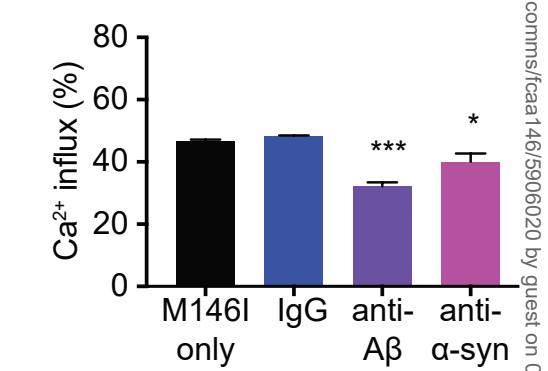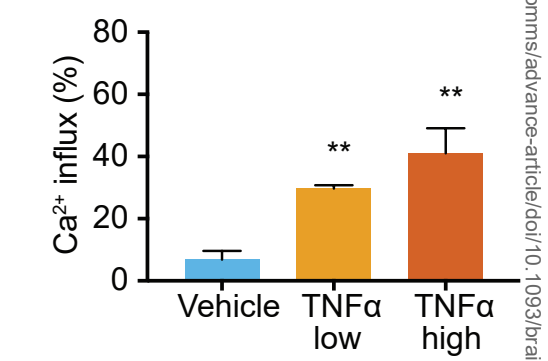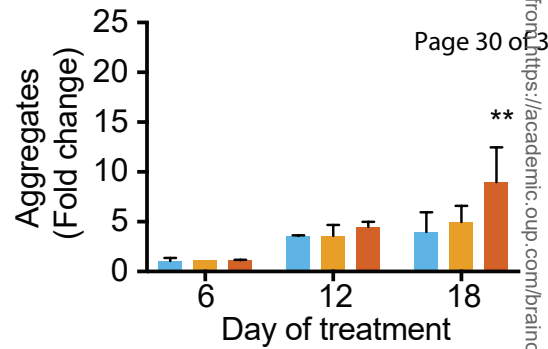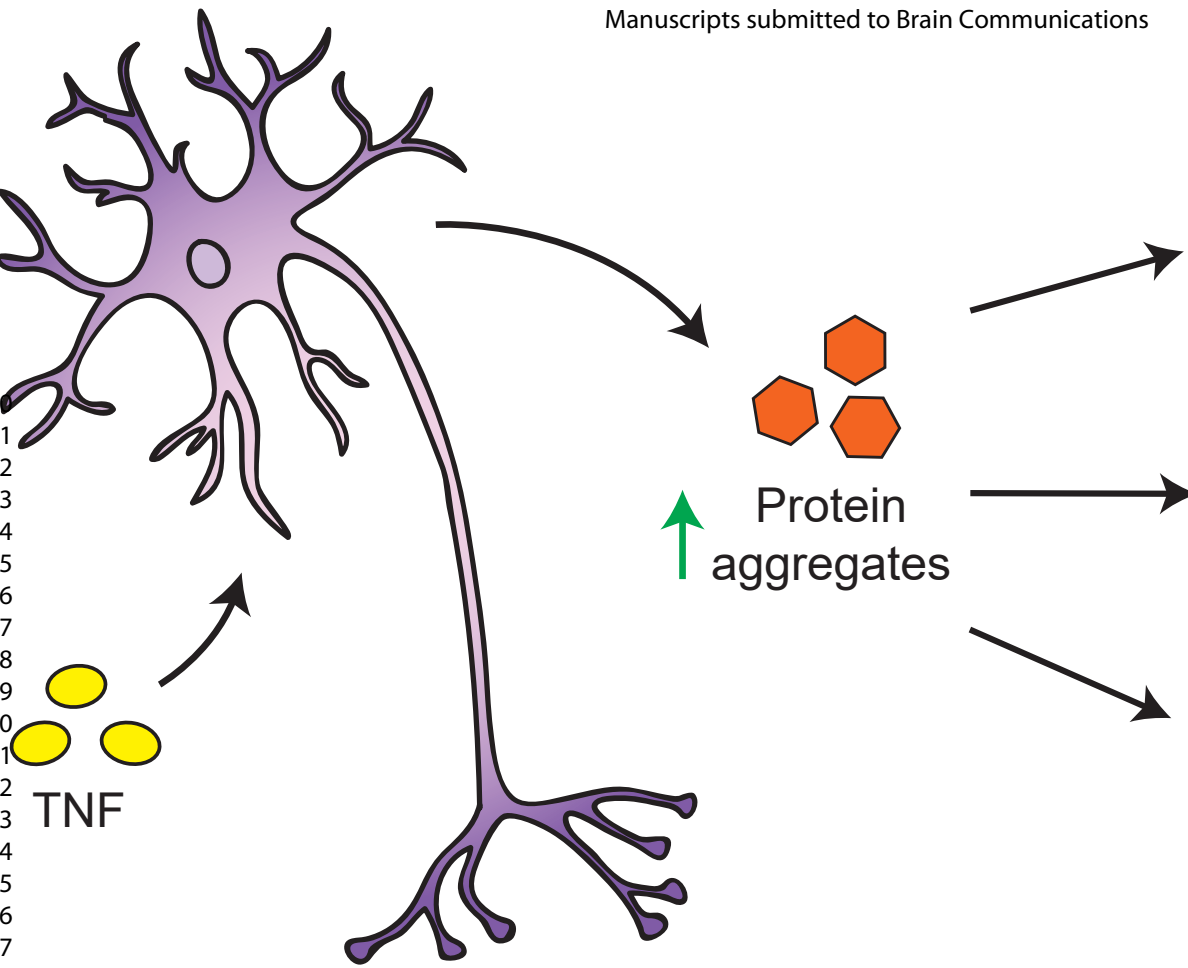
Abbreviated Summary

There is a complex interplay between neuroinflammation and protein aggregation in Alzheimer's disease. We show that chronic exposure to the inflammatory cytokine TNF stimulates monogenic Alzheimer's disease neurons to produce significantly more toxic protein aggregates, with no effect on healthy neurons, indicating a causal relationship between neuroinflammation and protein aggregation.